Proceedings of the
Annual Stability Conference
Structural Stability Research Council
Toronto, Canada, March 25-28, 2014

A new analytical method for solving nonlinear stability problems of framed structures

K.K.F. Wong[1]

Abstract
The traditional method of structural analysis with material nonlinearity has always been using the method of changing stiffness to capture the force reduction after yielding in the structure. This often raises a stability question on using the appropriate stiffness matrix to represent both geometric nonlinearity and material nonlinearity – How will the axial force on the column affect the tangent stiffness of the plastic hinges and the moment-resisting frame? In this research, the force analogy method combined with the stability functions will be used to answer this question. Through this unique combination, the stiffness force is computed by simply multiplying a nonlinear stiffness matrix (due to geometric nonlinearity using stability functions) with a nonlinear displacement vector (due to material nonlinearity using the force analogy method). A detailed derivation of the nonlinear stiffness matrices taking into consideration both geometric and material nonlinearities is here presented to demonstrate the simplicity of the combined method in addressing the nonlinear coupling effect.

1. Introduction

Buildings constructed in seismic regions are expected to experience significant deformation during a major earthquake. While design codes and standards have been developed to establish the seismic capacity for the structural design, estimating the seismic demand in nonlinear structures has always been a challenging task because no analytical theory exists in capturing the response of structures with significant geometric nonlinearity coupled with significant material nonlinearity, such as in the case of near-structural collapse. Engineers often rely on numerical methods and software subroutines to handle this coupling effect of nonlinearities, but software developers typically use their knowledge and preferences to make independent assumptions on what are best for their algorithms. One good example is that Perform-3D (CSI 2011a) uses P-Δ stiffness matrix and SAP2000 (CSI 2011b) uses the geometric stiffness matrix to address geometric nonlinearity effects. The end result is that there is a lack of consistency in the outputs between software packages for addressing nonlinearities, which can often go back and attribute it to the lack of analytical theory in handling the coupling effect.

In this research, an analytical method of handling the coupling effect of nonlinearities is

[1] Research Structural Engineer, National Institute of Standards and Technology, <kfwong@nist.gov>

developed through the combination of the force analogy method for handling material nonlinearity with the stability functions for handling geometric nonlinearity. Here, the force analogy method uses the initial stiffness with changing displacements in the formulation of material nonlinearity to quantify the stiffness force in the structure. Because the stiffness matrices remain unchanged with material nonlinearity, geometric nonlinearity using stability functions can easily be incorporated into the formulation by updating the geometric stiffness matrices due to changes in axial forces in the column members. The end result is that the stiffness force is computed by simply multiplying a nonlinear stiffness matrix with a nonlinear displacement vector.

In this paper, a detailed formulation on the nonlinear stiffness matrices taking into consideration both geometric and material nonlinearities is first derived for a column member. Once these stiffness matrices are assembled to form the global stiffness matrices, several examples are then followed to demonstrate the simplicity of the method for analyzing nonlinear framed structures.

2. Force Analogy Method

The Force Analogy Method (FAM) is a tool for calculating the internal forces and deformations of a material nonlinear structure due to the applied forces. The detailed derivation of the FAM has been presented in Wong and Yang (1999), and it is here briefly discussed with the inclusion of geometric nonlinear effects. Consider a moment-resisting frame with *n* degrees of freedom (DOFs) and *m* plastic hinge locations (PHLs). Let the total displacement $\mathbf{x}$ at each DOF be represented as the summation of elastic displacement $\mathbf{x}'$ and inelastic displacement $\mathbf{x}''$:

$$\mathbf{x} = \mathbf{x}' + \mathbf{x}'' \tag{1}$$

Similarly, let the total moment $\mathbf{M}$ at the PHLs of a moment-resisting frame be separated into elastic moment $\mathbf{M}'$ and inelastic moment $\mathbf{M}''$:

$$\mathbf{M} = \mathbf{M}' + \mathbf{M}'' \tag{2}$$

The displacements in Eq. 1 and the moments in Eq. 2 are related by the equations:

$$\mathbf{M}' = \mathbf{K}'^{T}\mathbf{x}' \quad , \quad \mathbf{M}'' = -\left[\mathbf{K}'' - \mathbf{K}'^{T}\mathbf{K}^{-1}\mathbf{K}'\right]\boldsymbol{\Theta}'' \quad , \quad \mathbf{x}'' = \mathbf{K}^{-1}\mathbf{K}'\boldsymbol{\Theta}'' \tag{3}$$

where $\boldsymbol{\Theta}''$ is the plastic rotation at the PHLs, $\mathbf{K}$ is the $n \times n$ global stiffness matrix, $\mathbf{K}'$ is the $n \times m$ assembled stiffness matrix relating plastic rotations at the PHLs and forces at the DOFs, and $\mathbf{K}''$ is the $m \times m$ assembled stiffness matrix relating plastic rotations with corresponding moments at the PHLs. For the *i*th beam or column member of the structure with plastic hinges at both ends but subjected to no axial force (or when geometric nonlinearity is ignored), the element stiffness matrices relating the shear and moment with deformations can be written as:

$$\mathbf{K}_i = \frac{EI}{L^3}\left[\begin{array}{cc:cc} 12 & 6L & -12 & 6L \\ 6L & 4L^2 & -6L & 2L^2 \\ \hdashline -12 & -6L & 12 & -6L \\ 6L & 2L^2 & -6L & 4L^2 \end{array}\right] \quad , \quad \mathbf{K}'_i = \frac{EI}{L^2}\left[\begin{array}{cc} 6 & 6 \\ 4L & 2L \\ \hdashline -6 & -6 \\ 2L & 4L \end{array}\right] \quad , \quad \mathbf{K}''_i = \frac{EI}{L}\begin{bmatrix} 4 & 2 \\ 2 & 4 \end{bmatrix} \tag{4}$$

Through matrix manipulations, the governing equation of the FAM due to an external applied force $\mathbf{F}_a$ can be written as

$$\left[\begin{array}{c|c} \mathbf{K} & \mathbf{K}' \\ \hline \mathbf{K}'^T & \mathbf{K}'' \end{array}\right]\left\{\begin{array}{c} \mathbf{x} \\ \hline -\boldsymbol{\Theta}'' \end{array}\right\} = \left\{\begin{array}{c} \mathbf{F}_a \\ \hline \mathbf{M} \end{array}\right\} \tag{5}$$

3. Stability Functions

To incorporate geometric nonlinearity into the analysis with material nonlinearity based on the FAM, the stiffness matrices $\mathbf{K}_i$, $\mathbf{K}'_i$, and $\mathbf{K}''_i$ of the *i*th column member in Eq. 4 must be derived by taking into consideration the axial compressive force on the member. Some of the previous derivations of the *i*th member elastic stiffness matrix $\mathbf{K}_i$ (McGuire et al. 2000, Wilson 2002, Powell 2010) include the *P*-Δ and geometric stiffness approaches, where the stiffness matrix for the *P*-Δ approach (i.e., $\mathbf{K}_{i(P\Delta)}$) and that for the geometric stiffness approach (i.e., $\mathbf{K}_{i(GS)}$) are

$$\mathbf{K}_{i(P\Delta)} = \frac{EI}{L^3}\begin{bmatrix} 12 & 6L & -12 & 6L \\ 6L & 4L^2 & -6L & 2L^2 \\ -12 & -6L & 12 & -6L \\ 6L & 2L^2 & -6L & 4L^2 \end{bmatrix} + \frac{P}{L}\begin{bmatrix} -1 & 0 & 1 & 0 \\ 0 & 0 & 0 & 0 \\ 1 & 0 & -1 & 0 \\ 0 & 0 & 0 & 0 \end{bmatrix} \tag{6}$$

$$\mathbf{K}_{i(GS)} = \frac{EI}{L^3}\begin{bmatrix} 12 & 6L & -12 & 6L \\ 6L & 4L^2 & -6L & 2L^2 \\ -12 & -6L & 12 & -6L \\ 6L & 2L^2 & -6L & 4L^2 \end{bmatrix} + \frac{P}{L}\begin{bmatrix} -6/5 & -L/10 & 6/5 & -L/10 \\ -L/10 & -2L^2/15 & L/10 & L^2/30 \\ 6/5 & L/10 & -6/5 & L/10 \\ -L/10 & L^2/30 & L/10 & -2L^2/15 \end{bmatrix} \tag{7}$$

The stability theory of using stability functions, on the other hand, was developed for elastic structures in the 1960's (Timoshenko and Gere 1961, Horne and Merchant 1965, Bazant and Cedolin 2003), but it found limited applications because of its complexity in the closed-form solution as compared to those using either the *P*-Δ approach in Eq. 6 or the geometric stiffness approach in Eq. 7. Even with the advance in computing technology, only one research publication was found in the recent literature on the analysis of framed structures using stability functions (Park and Kim 2008). For structures with significant lateral deflection, large geometric nonlinearity is expected, and linear or second-order approximation of the geometric stiffness may not be able to capture the nonlinear behavior accurately. Therefore, stability functions are here used to incorporate with the FAM to analyze structures with both geometric and material nonlinearities.

Although the theory of using stability functions in analyzing elastic frame buckling has been fully developed half a century ago, the derivation of *i*th member elastic stiffness matrix $\mathbf{K}_i$ is repeated here mainly because this derivation is important to the subsequent derivations of inelastic $\mathbf{K}'_i$ and $\mathbf{K}''_i$ matrices. While recognizing that only column members will be subjected to the axial compression and beam members will experience insignificant axial force due to the presence of the slab, the columns are rotated 90° in the following derivation of the stiffness matrices using the classical beam theory with an applied axial compressive load. Therefore the word 'beam' will be used interchangeably with the word 'column' in this section.

3.1 Stiffness Matrix [$\mathbf{K}_i$ *]*

Consider separately the four cases of a beam deflection subjected to various displacement patterns as shown in Fig. 1 in deriving the stiffness matrices. Here, V_{1l}, M_{1l}, V_{2l}, and M_{2l} represent the fixed-end shears and moments of the beam, and $l = 1,...,4$ represents the four cases of unit displacement patterns of beam deflection.

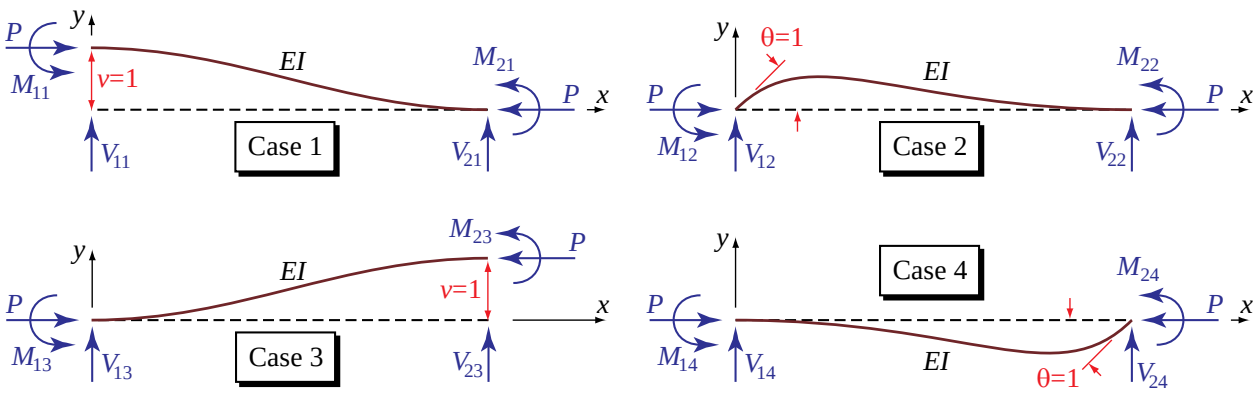

Figure 1: Displacement patterns and the corresponding fixed-end forces

Using the classical Bernoulli-Euler beam theory where the moment is proportional to the curvature, the governing equilibrium equation describing the deflected shape of the beam member can be written as

$$(EIv'')'' + Pv'' = 0 \tag{8}$$

where E is the elastic modulus, I is the moment of inertia, v is the lateral deflection, P is the axial compressive force of the member, and each prime represents taking derivatives of the corresponding variable with respect to the x-direction of the member. By assuming EI is constant along the member, the solution to the fourth-order ordinary differential equation becomes:

$$v = A\sin kx + B\cos kx + Cx + D \tag{9}$$

where $k^2 = P/EI$. Let $\lambda = kL$ to simplify the derivations, where L is the length of the member. The following four cases of boundary conditions (not in numerical order) are now considered.

Case 2: Imposing the boundary conditions $v(0) = 0$, $v'(0) = 1$, $v(L) = 0$, and $v'(L) = 0$ gives

$$v(0) = 0: \qquad B + D = 0 \tag{10a}$$
$$v'(0) = 1: \qquad kA + C = 1 \tag{10b}$$
$$v(L) = 0: \qquad A\sin\lambda + B\cos\lambda + CL + D = 0 \tag{10c}$$
$$v'(L) = 0: \qquad kA\cos\lambda - kB\sin\lambda + C = 0 \tag{10d}$$

Solving simultaneously for the constants in Eq. 10 gives

$$A = \frac{L(\lambda\sin\lambda + \cos\lambda - 1)}{\lambda(\lambda\sin\lambda + 2\cos\lambda - 2)}, \quad B = \frac{L(\lambda\cos\lambda - \sin\lambda)}{\lambda(\lambda\sin\lambda + 2\cos\lambda - 2)}, \quad C = 1 - kA, \quad D = -B \tag{11}$$

Therefore, Eq. 9 along with the constants in Eq. 11 gives the deflected shape for Case 2. The shears and moments at the two ends of the member (see Fig. 1) are then evaluated using the classical beam theory formula:

$$M(x) = EIv'' \quad , \quad V(x) = EIv''' + Pv' \tag{12}$$

Substituting Eq. 9 into Eq. 12 and using the constants calculated in Eq. 11, the fixed-end forces as labeled in Fig. 1 (Case 2) are calculated as:

$$M_{12} = -EIv''(0) = EIk^2 B = sEI/L \tag{13a}$$
$$V_{12} = EIv'''(0) + Pv'(0) = -EIk^3 A + P \times 1 = \bar{s}EI/L^2 \tag{13b}$$
$$M_{22} = EIv''(L) = -EIk^2\left(A\sin\lambda + B\cos\lambda\right) = scEI/L \tag{13c}$$
$$V_{22} = -EIv'''(L) - Pv'(L) = EIk^3\left(A\cos\lambda - B\sin\lambda\right) - P \times 0 = -\bar{s}EI/L^2 \tag{13d}$$

where

$$s = \frac{\lambda\left(\sin\lambda - \lambda\cos\lambda\right)}{2 - 2\cos\lambda - \lambda\sin\lambda} \quad , \quad c = \frac{\lambda - \sin\lambda}{\sin\lambda - \lambda\cos\lambda} \quad , \quad \bar{s} = s + sc = \frac{\lambda^2\left(1 - \cos\lambda\right)}{2 - 2\cos\lambda - \lambda\sin\lambda} \tag{14}$$

The minus signs in front of the calculations for M_{12} in Eq. 13a and V_{22} in Eq. 13d appear because of the differences in sign convention between the classical beam theory and the theory for stiffness method of structural analysis.

Case 4: Imposing the boundary conditions $v(0) = 0$, $v'(0) = 0$, $v(L) = 0$, and $v'(L) = 1$ gives

$$v(0) = 0: \qquad B + D = 0 \tag{15a}$$
$$v'(0) = 0: \qquad kA + C = 0 \tag{15b}$$
$$v(L) = 0: \qquad A\sin\lambda + B\cos\lambda + CL + D = 0 \tag{15c}$$
$$v'(L) = 1: \qquad kA\cos\lambda - kB\sin\lambda + C = 1 \tag{15d}$$

Solving simultaneously for the constants in Eq. 15 gives

$$A = \frac{L\left(1 - \cos\lambda\right)}{\lambda\left(\lambda\sin\lambda + 2\cos\lambda - 2\right)} \quad , \quad B = \frac{L\left(\sin\lambda - \lambda\right)}{\lambda\left(\lambda\sin\lambda + 2\cos\lambda - 2\right)} \quad , \quad C = -kA \quad , \quad D = -B \tag{16}$$

These constants in Eq. 16 are used to give the deflected shape in Eq. 9 for Case 4. Now substituting Eq. 9 into Eq. 12 and using the constants calculated in Eq. 16, the fixed-end forces as labeled in Fig. 1 (Case 4) are calculated as:

$$M_{14} = -EIv''(0) = EIk^2 B = scEI/L \tag{17a}$$
$$V_{14} = EIv'''(0) + Pv'(0) = -EIk^3 A + P \times 0 = \bar{s}EI/L^2 \tag{17b}$$
$$M_{24} = EIv''(L) = -EIk^2\left(A\sin\lambda + B\cos\lambda\right) = sEI/L \tag{17c}$$
$$V_{24} = -EIv'''(L) - Pv'(L) = EIk^3\left(A\cos\lambda - B\sin\lambda\right) - P \times 1 = -\bar{s}EI/L^2 \tag{17d}$$

where s, c, and $\bar{s}$ are given in Eq. 14.

Case 1: Imposing the boundary conditions $v(0)=1$, $v'(0)=0$, $v(L)=0$, and $v'(L)=0$ gives

$$v(0)=1: \qquad B+D=1 \tag{18a}$$
$$v'(0)=0: \qquad kA+C=0 \tag{18b}$$
$$v(L)=0: \qquad A\sin\lambda+B\cos\lambda+CL+D=0 \tag{18c}$$
$$v'(L)=0: \qquad kA\cos\lambda-kB\sin\lambda+C=0 \tag{18d}$$

Solving simultaneously for the constants in Eq. 18 gives

$$A=\frac{\sin\lambda}{\lambda\sin\lambda+2\cos\lambda-2} \quad , \quad B=\frac{\cos\lambda-1}{\lambda\sin\lambda+2\cos\lambda-2} \quad , \quad C=-kA \quad , \quad D=1-B \tag{19}$$

These constants in Eq. 19 are used to give the deflected shape in Eq. 9 for Case 1. Now substituting Eq. 9 into Eq. 12 and using the constants calculated in Eq. 19, the fixed-end forces as labeled in Fig. 1 (Case 1) are calculated as:

$$M_{11}=-EIv''(0)=EIk^2B=\bar{s}EI/L^2 \tag{20a}$$
$$V_{11}=EIv'''(0)+Pv'(0)=-EIk^3A+P\times 0=s'EI/L^3 \tag{20b}$$
$$M_{21}=EIv''(L)=-EIk^2\left(A\sin\lambda+B\cos\lambda\right)=\bar{s}EI/L^2 \tag{20c}$$
$$V_{21}=-EIv'''(L)-Pv'(L)=EIk^3\left(A\cos\lambda-B\sin\lambda\right)-P\times 0=-s'EI/L^3 \tag{20d}$$

where

$$s'=2\bar{s}-\lambda^2=\frac{\lambda^3\sin\lambda}{2-2\cos\lambda-\lambda\sin\lambda} \tag{21}$$

and $\bar{s}$ is given in Eq. 14.

Case 3: Imposing the boundary conditions $v(0)=0$, $v'(0)=0$, $v(L)=1$, and $v'(L)=0$ gives

$$v(0)=0: \qquad B+D=0 \tag{22a}$$
$$v'(0)=0: \qquad kA+C=0 \tag{22b}$$
$$v(L)=1: \qquad A\sin\lambda+B\cos\lambda+CL+D=1 \tag{22c}$$
$$v'(L)=0: \qquad kA\cos\lambda-kB\sin\lambda+C=0 \tag{22d}$$

Solving simultaneously for the constants in Eq. 22 gives

$$A=-\frac{\sin\lambda}{\lambda\sin\lambda+2\cos\lambda-2} \quad , \quad B=\frac{1-\cos\lambda}{\lambda\sin\lambda+2\cos\lambda-2} \quad , \quad C=-kA \quad , \quad D=-B \tag{23}$$

These constants in Eq. 23 are used to give the deflected shape in Eq. 9 for Case 3. Now substituting Eq. 9 into Eq. 12 and using the constants calculated in Eq. 23, the fixed-end forces as

labeled in Fig. 1 (Case 3) are calculated as:

$$M_{13} = -EIv''(0) = EIk^2 B = -\bar{s}EI/L^2 \tag{24a}$$
$$V_{13} = EIv'''(0) + Pv'(0) = -EIk^3 A + P \times 0 = -s'EI/L^3 \tag{24b}$$
$$M_{23} = EIv''(L) = -EIk^2\left(A\sin\lambda + B\cos\lambda\right) = -\bar{s}EI/L^2 \tag{24c}$$
$$V_{23} = -EIv'''(L) - Pv'(L) = EIk^3\left(A\cos\lambda - B\sin\lambda\right) - P \times 0 = s'EI/L^3 \tag{24d}$$

where $\bar{s}$ is given in Eq. 14 and s' is given in Eq. 21.

In summary, based on Eqs. 13, 17, 20, and 24 for the above four cases, the stiffness matrix of the *i*th member $\mathbf{K}_{i(SF)}$ after incorporating axial compressive force using stability functions becomes:

$$\mathbf{K}_{i(SF)} = \frac{EI}{L^3}\begin{bmatrix} s' & \bar{s}L & -s' & \bar{s}L \\ \bar{s}L & sL^2 & -\bar{s}L & scL^2 \\ -s' & -\bar{s}L & s' & -\bar{s}L \\ \bar{s}L & scL^2 & -\bar{s}L & sL^2 \end{bmatrix} \begin{matrix} \leftarrow v(0) \\ \leftarrow v'(0) \\ \leftarrow v(L) \\ \leftarrow v'(L) \end{matrix} \tag{25}$$

3.2 Stiffness Matrix [$\mathbf{K}_i'$]

The stiffness matrix $\mathbf{K}_i'$ relates the plastic rotations at the PHLs with the restoring forces applied at the DOFs. However, computing the restoring forces at the two ends of the member due to a unit plastic rotation at the PHL is a difficult process. To avoid this problem, the $\mathbf{K}_i'^T$ matrix relating the displacements at the two ends of the member with the moments at the PHLs is constructed.

Consider the four cases of unit displacements of the beam member as shown in Fig. 2, where the moment at the plastic hinges '*a*' and '*b*' (i.e., M_{al} and M_{bl}, $l = 1,...,4$) represent the desired quantities. Note that the fixed end moments (i.e., M_{1l} and M_{2l}, $l = 1,...,4$) have already been calculated and summarized in the second and fourth rows of the stiffness matrix given in Eq. 25. Based on Fig. 2, the moments at the two plastic hinges for each of the four cases become:

Case 1: Imposing the boundary conditions $v(0) = 1$, $v'(0) = 0$, $v(L) = 0$, and $v'(L) = 0$ gives

$$M_{a1} = M_{11} = \bar{s}EI/L^2 \quad , \quad M_{b1} = M_{21} = \bar{s}EI/L^2 \tag{26}$$

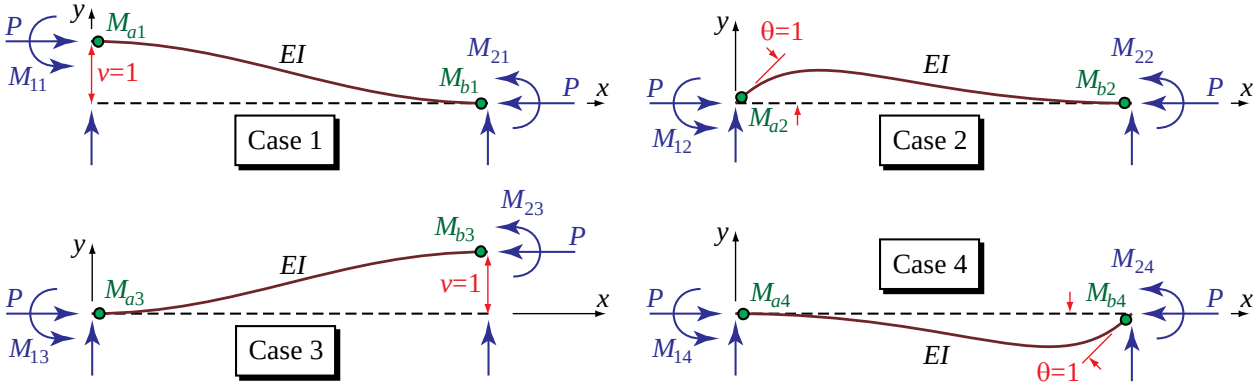

Figure 2: Displacement patterns for computation of moments at the plastic hinge locations

Case 2: Imposing the boundary conditions $v(0)=0$, $v'(0)=1$, $v(L)=0$, and $v'(L)=0$ gives

$$M_{a2}=M_{12}=sEI/L \quad , \quad M_{b2}=M_{22}=scEI/L \tag{27}$$

Case 3: Imposing the boundary conditions $v(0)=0$, $v'(0)=0$, $v(L)=1$, and $v'(L)=0$ gives

$$M_{a3}=M_{13}=-\bar{s}EI/L^2 \quad , \quad M_{b3}=M_{23}=-\bar{s}EI/L^2 \tag{28}$$

Case 4: Imposing the boundary conditions $v(0)=0$, $v'(0)=0$, $v(L)=0$, and $v'(L)=1$ gives

$$M_{a4}=M_{14}=scEI/L \quad , \quad M_{b4}=M_{24}=sEI/L \tag{29}$$

From Eqs. 26 to 29, the transpose of stiffness matrix $\mathbf{K}_i'$ for the *i*th member becomes

$$\mathbf{K}_i'^{T}=\begin{bmatrix} \bar{s}EI/L^2 & sEI/L & -\bar{s}EI/L^2 & scEI/L \\ \bar{s}EI/L^2 & scEI/L & -\bar{s}EI/L^2 & sEI/L \end{bmatrix} \begin{matrix} \leftarrow \theta_a'' \\ \leftarrow \theta_b'' \end{matrix} \tag{30}$$

Once the $\mathbf{K}_i'^{T}$ matrix in Eq. 30 is derived, the $\mathbf{K}_i'$ matrix can be written as:

$$\mathbf{K}_i'=\begin{bmatrix} M_{a1} & M_{b1} \\ M_{a2} & M_{b2} \\ M_{a3} & M_{b3} \\ M_{a4} & M_{b4} \end{bmatrix}=\begin{bmatrix} \bar{s}EI/L^2 & \bar{s}EI/L^2 \\ sEI/L & scEI/L \\ -\bar{s}EI/L^2 & -\bar{s}EI/L^2 \\ scEI/L & sEI/L \end{bmatrix} \begin{matrix} \leftarrow v(0) \\ \leftarrow v'(0) \\ \leftarrow v(L) \\ \leftarrow v'(L) \end{matrix} \tag{31}$$

3.3 Stiffness Matrix [$\mathbf{K}_i''$]

The stiffness matrix $\mathbf{K}_i''$ relates the moments at the PHLs with a corresponding unit plastic rotation at each PHL. To determine the $\mathbf{K}_i''$ matrix, the goal is to compute M_{aa}, M_{ab}, M_{ba}, and M_{bb} as shown in Fig. 3.

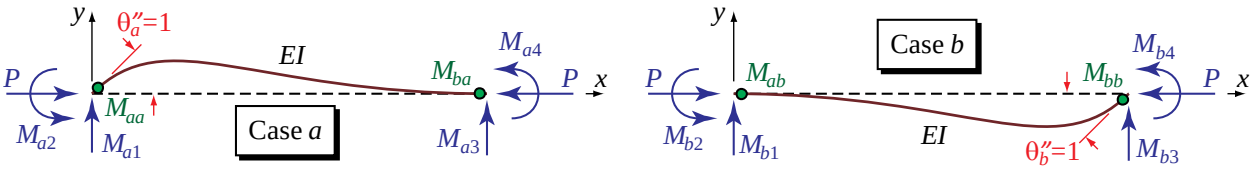

Figure 3: Displacement patterns for computation of moments due to unit plastic rotations

The fixed-end forces evaluated in the $\mathbf{K}_i'$ matrix can be used to calculate the stiffness matrix $\mathbf{K}_i''$. For example, the first column of the 4×2 $\mathbf{K}_i'$ matrix in Eq. 31 represents the fixed-end shears (M_{a1} and M_{a3}) and moments (M_{a2} and M_{a4}) of the beam member due to a unit plastic rotation at the left plastic hinge (i.e., PHL '*a*'), as shown in Fig. 3. Similarly, the second column of the 4×2 $\mathbf{K}_i'$ matrix in Eq. 31 represents the fixed-end shears (M_{b1} and M_{b3}) and moments (M_{b2} and M_{b4}) of the beam member due to a unit plastic rotation at the right plastic hinge (i.e., PHL '*b*'), as shown in Fig. 3. Then the moments at the two plastic hinges for each of the two cases can be evaluated as:

Case '*a*': Imposing a unit plastic rotation $\theta''_a = 1$ and $\theta''_b = 0$ gives

$$M_{aa} = M_{a2} = sEI/L \quad , \quad M_{ba} = M_{a4} = scEI/L \tag{32}$$

Case '*b*': Imposing a unit plastic rotation $\theta''_a = 0$ and $\theta''_b = 1$ gives

$$M_{ab} = M_{b2} = scEI/L \quad , \quad M_{bb} = M_{b4} = sEI/L \tag{33}$$

From Eqs. 32 and 33, the stiffness matrix $\mathbf{K}''_i$ for the *i*th member becomes

$$\mathbf{K}''_i = \begin{bmatrix} sEI/L & scEI/L \\ scEI/L & sEI/L \end{bmatrix} \begin{matrix} \leftarrow \theta''_a \\ \leftarrow \theta''_b \end{matrix} \tag{34}$$

4. Advantage of Using Stability Functions

Consider a beam member of length $3L$ with elastic modulus E and moment of inertia I subjected to an axial compressive force $P = 0.2 \times EI/L^2$ as shown in Fig. 4. Following Eqs. 6, 7, and 25, the element stiffness matrices $\mathbf{K}_i$ using DOFs #1 to #4 with geometric nonlinearity considered can be written as

$$\mathbf{K}_{i(P\Delta)} = \frac{EI}{L^3}\begin{bmatrix} 0.37778 & 0.66667L & -0.37778 & 0.66667L \\ 0.66667L & 1.33333L^2 & -0.66667L & 0.66667L^2 \\ -0.37778 & -0.66667L & 0.37778 & -0.66667L \\ 0.66667L & 0.66667L^2 & -0.66667L & 1.33333L^2 \end{bmatrix} \begin{matrix} \leftarrow \text{DOF\#1} \\ \leftarrow \text{DOF\#2} \\ \leftarrow \text{DOF\#3} \\ \leftarrow \text{DOF\#4} \end{matrix} \tag{35a}$$

$$\mathbf{K}_{i(GS)} = \frac{EI}{L^3}\begin{bmatrix} 0.36444 & 0.64667L & -0.36444 & 0.64667L \\ 0.64667L & 1.25333L^2 & -0.64667L & 0.68667L^2 \\ -0.36444 & -0.64667L & 0.36444 & -0.64667L \\ 0.64667L & 0.68667L^2 & -0.64667L & 1.25333L^2 \end{bmatrix} \begin{matrix} \leftarrow \text{DOF\#1} \\ \leftarrow \text{DOF\#2} \\ \leftarrow \text{DOF\#3} \\ \leftarrow \text{DOF\#4} \end{matrix} \tag{35b}$$

$$\mathbf{K}_{i(SF)} = \begin{bmatrix} 0.36427 & 0.64640L & -0.36427 & 0.64640L \\ 0.64640L & 1.25137L^2 & -0.64640L & 0.68784L^2 \\ -0.36427 & -0.64640L & 0.36427 & -0.64640L \\ 0.64640L & 0.68784L^2 & -0.64640L & 1.25137L^2 \end{bmatrix} \begin{matrix} \leftarrow \text{DOF\#1} \\ \leftarrow \text{DOF\#2} \\ \leftarrow \text{DOF\#3} \\ \leftarrow \text{DOF\#4} \end{matrix} \tag{35c}$$

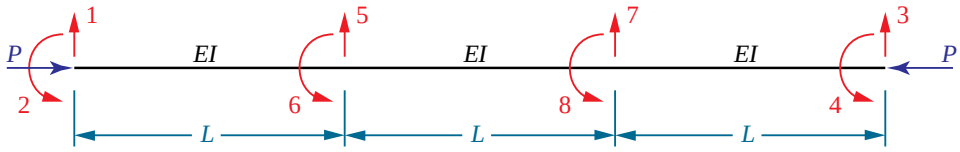

Figure 4: Beam member subdivided into three elements

Now assume that the same member is subdivided into three elements of equal lengths L. The stiffness matrices using DOFs #1 to #8 as labeled in Fig. 4 with geometric nonlinearity considered can be written as

$$\mathbf{K}_{P\Delta} = \frac{EI}{L^3}\left[\begin{array}{cccc:cccc} 11.8 & 6L & 0 & 0 & -11.8 & 6L & 0 & 0 \\ 6L & 4L^2 & 0 & 0 & -6L & 2L^2 & 0 & 0 \\ 0 & 0 & 11.8 & -6L & 0 & 0 & -11.8 & -6L \\ 0 & 0 & -6L & 4L^2 & 0 & 0 & 6L & 2L^2 \\ \hdashline -11.8 & -6L & 0 & 0 & 23.6 & 0 & -11.8 & 6L \\ 6L & 2L^2 & 0 & 0 & 0 & 8L^2 & -6L & 2L^2 \\ 0 & 0 & -11.8 & 6L & -11.8 & -6L & 23.6 & 0 \\ 0 & 0 & -6L & 2L^2 & 6L & 2L^2 & 0 & 8L^2 \end{array}\right] \begin{array}{l} \leftarrow \text{DOF\#1} \\ \leftarrow \text{DOF\#2} \\ \leftarrow \text{DOF\#3} \\ \leftarrow \text{DOF\#4} \\ \\ \leftarrow \text{DOF\#5} \\ \leftarrow \text{DOF\#6} \\ \leftarrow \text{DOF\#7} \\ \leftarrow \text{DOF\#8} \end{array} \tag{36a}$$

$$\mathbf{K}_{GS} = \frac{EI}{L^3}\left[\begin{array}{cccc:cccc} 11.76 & 5.98L & 0 & 0 & -11.76 & 5.98L & 0 & 0 \\ 5.98L & 3.97L^2 & 0 & 0 & -5.98L & 2.01L^2 & 0 & 0 \\ 0 & 0 & 11.76 & -5.98L & 0 & 0 & -11.76 & -5.98L \\ 0 & 0 & -5.98L & 3.97L^2 & 0 & 0 & 5.98L & 2.01L^2 \\ \hdashline -11.76 & -5.98L & 0 & 0 & 23.52 & 0 & -11.76 & 5.98L \\ 5.98L & 2.01L^2 & 0 & 0 & 0 & 7.95L^2 & -5.98L & 2.01L^2 \\ 0 & 0 & -11.76 & 5.98L & -11.76 & -5.98L & 23.52 & 0 \\ 0 & 0 & -5.98L & 2.01L^2 & 5.98L & 2.01L^2 & 0 & 7.95L^2 \end{array}\right] \tag{36b}$$

$$\mathbf{K}_{SF} = \frac{EI}{L^3}\left[\begin{array}{cccc:cccc} 11.76 & 5.98L & 0 & 0 & -11.76 & 5.98L & 0 & 0 \\ 5.98L & 3.97L^2 & 0 & 0 & -5.98L & 2.01L^2 & 0 & 0 \\ 0 & 0 & 11.76 & -5.98L & 0 & 0 & -11.76 & -5.98L \\ 0 & 0 & -5.98L & 3.97L^2 & 0 & 0 & 5.98L & 2.01L^2 \\ \hdashline -11.76 & -5.98L & 0 & 0 & 23.52 & 0 & -11.76 & 5.98L \\ 5.98L & 2.01L^2 & 0 & 0 & 0 & 7.95L^2 & -5.98L & 2.01L^2 \\ 0 & 0 & -11.76 & 5.98L & -11.76 & -5.98L & 23.52 & 0 \\ 0 & 0 & -5.98L & 2.01L^2 & 5.98L & 2.01L^2 & 0 & 7.95L^2 \end{array}\right] \tag{36c}$$

Note that $\mathbf{K}_{GS} \approx \mathbf{K}_{SF}$ within three significant digits.

Static condensation is now used to eliminate DOFs #5 to #8 from the stiffness matrices in Eq. 36 based on the equation

$$\overline{\mathbf{K}} = \mathbf{K}_{11} - \mathbf{K}_{12}\mathbf{K}_{22}^{-1}\mathbf{K}_{21} \tag{37}$$

where $\mathbf{K}_{11}$, $\mathbf{K}_{12}$, $\mathbf{K}_{21}$, and $\mathbf{K}_{22}$ are sub-matrices partitioned according to the dotted lines of those full stiffness matrices shown in Eq. 36. It can be seen that each of these sub-matrices are 4×4 matrix, with subscript '2' denoting DOFs #5 to #8 to be condensed out and subscript '1' denoting DOFs #1 to #4 to be remained after condensation. Now substituting these sub-matrices presented in Eq. 36 into Eq. 37 and performing the matrix multiplications gives

$$\overline{\mathbf{K}}_{i(P\Delta)} = \frac{EI}{L^3}\begin{bmatrix} 0.37107 & 0.65660L & -0.37107 & 0.65660L \\ 0.65660L & 1.27226L^2 & -0.65660L & 0.69755L^2 \\ -0.37107 & -0.65660L & 0.37107 & -0.65660L \\ 0.65660L & 0.69755L^2 & -0.65660L & 1.27226L^2 \end{bmatrix} \begin{matrix} \leftarrow \text{DOF\#1} \\ \leftarrow \text{DOF\#2} \\ \leftarrow \text{DOF\#3} \\ \leftarrow \text{DOF\#4} \end{matrix} \tag{38a}$$

$$\overline{\mathbf{K}}_{i(GS)} = \frac{EI}{L^3}\begin{bmatrix} 0.36429 & 0.64644L & -0.36429 & 0.64644L \\ 0.64644L & 1.25144L^2 & -0.64644L & 0.68787L^2 \\ -0.36429 & -0.64644L & 0.36429 & -0.64644L \\ 0.64644L & 0.68787L^2 & -0.64644L & 1.25144L^2 \end{bmatrix} \begin{matrix} \leftarrow \text{DOF\#1} \\ \leftarrow \text{DOF\#2} \\ \leftarrow \text{DOF\#3} \\ \leftarrow \text{DOF\#4} \end{matrix} \tag{38b}$$

$$\overline{\mathbf{K}}_{i(SF)} = \frac{EI}{L^3}\begin{bmatrix} 0.36427 & 0.64640L & -0.36427 & 0.64640L \\ 0.64640L & 1.25137L^2 & -0.64640L & 0.68784L^2 \\ -0.36427 & -0.64640L & 0.36427 & -0.64640L \\ 0.64640L & 0.68784L^2 & -0.64640L & 1.25137L^2 \end{bmatrix} \begin{matrix} \leftarrow \text{DOF\#1} \\ \leftarrow \text{DOF\#2} \\ \leftarrow \text{DOF\#3} \\ \leftarrow \text{DOF\#4} \end{matrix} \tag{38c}$$

Comparing Eq. 35 with Eq. 38 shows that only the stability functions approach gives exactly the same stiffness matrix regardless of whether one long element is used or three subdivided elements are used. This indicates that while all three geometric nonlinearity approaches address large *P*-Δ appropriately, only stability functions approach captures small *P*-δ exactly. Note that the differences between the statically condensed matrices (i.e., $\overline{\mathbf{K}}_{i(P\Delta)}$ and $\overline{\mathbf{K}}_{i(GS)}$ relative to $\overline{\mathbf{K}}_{i(SF)}$ in Eq. 38) is smaller than those between the original matrices (i.e., $\mathbf{K}_{i(P\Delta)}$ and $\mathbf{K}_{i(GS)}$ relative to $\mathbf{K}_{i(SF)}$ in Eq. 35). This indicates that one way of capturing small *P*-δ effect in the *P*-Δ approach is to subdivide the member into several shorter elements.

5. Force Analogy Method with Stability Functions

Consider the one-story one-bay moment-resisting steel frame as shown in Fig. 5. Assume that axial deformation is ignored for all three members, this results in a system with 3 DOFs ($n = 3$) and 6 PHLs ($m = 6$) as labeled in the figure. Also assume that a lateral force of F_o is applied at the horizontal degree of freedom x_1, this gives $F_1 = F_o$ and $F_2 = F_3 = 0$.

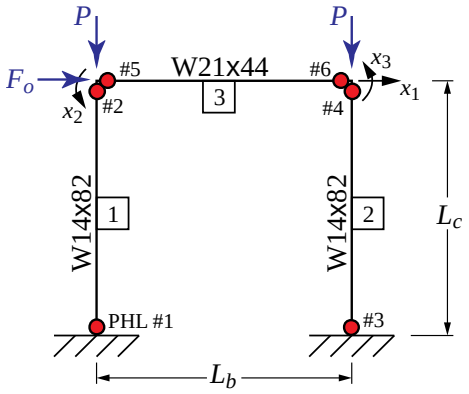

Figure 5: One-story one-bay moment-resisting steel frame

Since the axial force in Member 1 (denote as P_1) will be different from that of Member 2 (denote as P_2) due to overturning induced by the lateral applied force F_o, the resulting stability coefficients

will be different as well. The axial force in Member 3 is assumed to be negligible (i.e., $P_3 \approx 0$) due to the presence of slab, even though it is not explicitly modeled. Therefore, let

$$\lambda_1 = \sqrt{P_1/EI_c} \times L_c \quad , \quad \lambda_2 = \sqrt{P_2/EI_c} \times L_c \tag{39}$$

where $E = 29{,}000$ ksi for steel, and I_c is the moment of inertia and L_c is the length of the W14×82 columns. Also, let I_b be the moment of inertia and L_b be the length of the W21×44 beam. It then follows that the stiffness matrices of the FAM for this one-story frame become

$$\mathbf{K} = \begin{bmatrix} s_1' EI_c/L_c^3 + s_2' EI/L_c^3 & \bar{s}_1 EI_c/L_c^2 & \bar{s}_2 EI_c/L_c^2 \\ \bar{s}_1 EI_c/L_c^2 & s_1 EI_c/L_c + 4EI_b/L_b & 2EI_b/L_b \\ \bar{s}_2 EI_c/L_c^2 & 2EI_b/L_b & s_2 EI_c/L_c + 4EI_b/L_b \end{bmatrix} \begin{matrix} \leftarrow x_1 \\ \leftarrow x_2 \\ \leftarrow x_3 \end{matrix} \tag{40a}$$

$$\mathbf{K}' = \left[\begin{array}{cc:cc:cc} \bar{s}_1 EI_c/L_c^2 & \bar{s}_1 EI_c/L_c^2 & \bar{s}_2 EI_c/L_c^2 & \bar{s}_2 EI_c/L_c^2 & 0 & 0 \\ s_1 c_1 EI_c/L_c & s_1 EI_c/L_c & 0 & 0 & 4EI_b/L_b & 2EI_b/L_b \\ 0 & 0 & s_2 c_2 EI_c/L_c & s_2 EI_c/L_c & 2EI_b/L_b & 4EI_b/L_b \end{array}\right] \begin{matrix} \leftarrow x_1 \\ \leftarrow x_2 \\ \leftarrow x_3 \end{matrix} \tag{40b}$$

$$\mathbf{K}'' = \left[\begin{array}{cc:cc:cc} s_1 EI_c/L_c & s_1 c_1 EI_c/L_c & 0 & 0 & 0 & 0 \\ s_1 c_1 EI_c/L_c & s_1 EI_c/L_c & 0 & 0 & 0 & 0 \\ \hdashline 0 & 0 & s_2 EI_c/L_c & s_2 c_2 EI_c/L_c & 0 & 0 \\ 0 & 0 & s_2 c_2 EI_c/L_c & s_2 EI_c/L_c & 0 & 0 \\ \hdashline 0 & 0 & 0 & 0 & 4EI_b/L_b & 2EI_b/L_b \\ 0 & 0 & 0 & 0 & 2EI_b/L_b & 4EI_b/L_b \end{array}\right] \begin{matrix} \leftarrow \theta_1'' \\ \leftarrow \theta_2'' \\ \leftarrow \theta_3'' \\ \leftarrow \theta_4'' \\ \leftarrow \theta_5'' \\ \leftarrow \theta_6'' \end{matrix} \tag{40c}$$

where s_1, c_1, $\bar{s}_1$, and s_1' are the stability coefficients of Member 1 as functions of λ_1 and P_1, and s_2, c_2, $\bar{s}_2$, and s_2' are the stability coefficients of Member 2 as functions of λ_2 and P_2. The governing equation of the FAM based on Eq. 5 becomes

$$\left[\begin{array}{c:c} \mathbf{K}(3\times 3) & \mathbf{K}'(3\times 6) \\ \hdashline \mathbf{K}'^{T}(6\times 3) & \mathbf{K}''(6\times 6) \end{array}\right] \left\{\begin{array}{c} x_1 \\ x_2 \\ x_3 \\ \hdashline -\theta_1'' \\ -\theta_2'' \\ -\theta_3'' \\ -\theta_4'' \\ -\theta_5'' \\ -\theta_6'' \end{array}\right\} = \left\{\begin{array}{c} F_o \\ 0 \\ 0 \\ \hdashline M_1 \\ M_2 \\ M_3 \\ M_4 \\ M_5 \\ M_6 \end{array}\right\} \tag{41}$$

Let the gravity load on the frame be $P = 200$ kips. Also, let $L_b = 20$ ft and $L_c = 14$ ft, and a yield stress of steel be $f_Y = 36$ ksi. Assume yield surface is determined through the interaction between axial force and moment with the relationships:

$$\text{Columns:} \quad \left(\frac{P_k}{f_Y A_c}\right)^2 + \left(\frac{M_k}{f_Y Z_c}\right)^2 \le 1 \quad , \quad k = 1,...,4 \tag{42a}$$

$$\text{Beam:} \quad \left|\frac{M_k}{f_Y Z_b}\right| \le 1 \quad , \quad k = 5,6 \tag{42b}$$

where A_c is the cross-sectional area and Z_c is the plastic section modulus of the columns, and Z_b is the plastic section modulus of the beam. Let the material exhibits elastic-plastic behavior. This gives the moment versus plastic rotation relationships for the 6 PHLs as

$$\textit{if} \quad \begin{cases} M_k \le M_{Yc,k} \\ M_k > M_{Yc,k} \end{cases} , \quad \textit{then} \quad \begin{cases} \theta_k'' = 0 \\ M_k = M_{Yc,k} \end{cases} \quad i = 1,2,3,4 \tag{43a}$$

$$\textit{if} \quad \begin{cases} M_i \le f_Y Z_b \\ M_i > f_Y Z_b \end{cases} , \quad \textit{then} \quad \begin{cases} \theta_i'' = 0 \\ M_i = f_Y Z_b \end{cases} \quad i = 5,6 \tag{43b}$$

where $M_{Yc,k}$ is the moment capacity of the kth column plastic hinge computed based on a specified axial compressive force and the yield surface equation given in Eq. 42a. A pushover curve is now constructed for the frame by taking the following steps.

Step 1: The frame is initially assumed to respond in the linearly elastic range i.e., $\theta_1'' = \theta_2'' = \theta_3'' = \theta_4'' = \theta_5'' = \theta_6'' = 0$. At an applied force of $F_o = 484.4$ kips and $P_1 = P_2 = 200$ kips, extracting the first three equations of Eq. 41 gives

$$\begin{bmatrix} 126.5 & 5411 & 5411 \\ 5411 & 1011300 & 203730 \\ 5411 & 203730 & 1011300 \end{bmatrix} \begin{Bmatrix} x_1 \\ x_2 \\ x_3 \end{Bmatrix} = \begin{Bmatrix} 484.4 \\ 0 \\ 0 \end{Bmatrix} \tag{44}$$

Solving for the displacements at the DOFs gives

$$x_1 = 6.189 \text{ in.} \quad , \quad x_2 = x_3 = -0.0276 \text{ rad} \tag{45}$$

Then substituting Eq. 45 back into the last six equations of Eq. 41 gives the moments

$$\begin{Bmatrix} M_1 \\ M_2 \\ M_3 \\ M_4 \\ M_5 \\ M_6 \end{Bmatrix} = \begin{bmatrix} 5411 & 305280 & 0 \\ 5411 & 603820 & 0 \\ 5411 & 0 & 305280 \\ 5411 & 0 & 603820 \\ 0 & 407450 & 203730 \\ 0 & 203730 & 407450 \end{bmatrix} \begin{Bmatrix} 6.189 \\ -0.0276 \\ -0.0276 \end{Bmatrix} = \begin{Bmatrix} 25{,}078 \\ 16{,}848 \\ 25{,}078 \\ 16{,}848 \\ -16{,}848 \\ -16{,}848 \end{Bmatrix} \tag{46}$$

At this point, both M_5 and M_6 reach the moment capacity of $f_Y Z_b = 16{,}848$ k-in. Based on the

setup of the frame as shown in Fig. 5, the column axial force can be updated by computing the shear force at the two ends of the beam member using equilibrium of the beam, i.e.,

$$P_1 = P + (M_5 + M_6)/L_b = 200 + (-16{,}838 - 16{,}838)/240 = 59.6 \text{ kips} \tag{47a}$$

$$P_2 = P - (M_5 + M_6)/L_b = 200 - (-16{,}838 - 16{,}838)/240 = 340.4 \text{ kips} \tag{47b}$$

Step 2u: The analysis continues with PHLs #5 and #6 yielded, i.e., $\theta_1'' = \theta_2'' = \theta_3'' = \theta_4'' = 0$. The lateral force is applied up to $F_o = 524.7$ kips. Rows 1, 2, 3, 8, and 9 are extracted from Eq. 41 with the updated information on the column axial forces obtained in Eq. 47:

$$\left[\begin{array}{ccc:cc} 126.5 & 5425 & 5397 & 0 & 0 \\ 5425 & 1014400 & 203730 & 407450 & 203730 \\ 5397 & 203730 & 1008100 & 203730 & 407450 \\ \hdashline 0 & 407450 & 203730 & 407450 & 203730 \\ 0 & 203730 & 407450 & 203730 & 407450 \end{array}\right] \left\{\begin{array}{c} x_1 \\ x_2 \\ x_3 \\ \hdashline -\theta_5'' \\ -\theta_6'' \end{array}\right\} = \left\{\begin{array}{c} 524.7 \\ 0 \\ 0 \\ \hdashline -16{,}848 \\ -16{,}848 \end{array}\right\} \tag{48}$$

Solving for the displacements at the DOFs and plastic rotations in Eq. 48 gives

$$x_1 = 7.557 \text{ in.} \;,\quad x_2 = x_3 = -0.0398 \text{ rad} \;,\quad \theta_5'' = -0.0122 \text{ rad} \;,\quad \theta_6'' = -0.0123 \text{ rad} \tag{49}$$

Then substituting Eq. 49 back into the last six equations of Eq. 41 gives the moments

$$\left\{\begin{array}{c} M_1 \\ M_2 \\ M_3 \\ M_4 \\ M_5 \\ M_6 \end{array}\right\} = \left[\begin{array}{ccccc} 5425 & 304490 & 0 & 0 & 0 \\ 5425 & 606970 & 0 & 0 & 0 \\ 5397 & 0 & 306080 & 0 & 0 \\ 5397 & 0 & 600650 & 0 & 0 \\ 0 & 407450 & 203730 & 407450 & 203730 \\ 0 & 203730 & 407450 & 203730 & 407450 \end{array}\right] \left\{\begin{array}{c} 7.557 \\ -0.0398 \\ -0.0398 \\ 0.01223 \\ 0.01229 \end{array}\right\} = \left\{\begin{array}{c} 28{,}884 \\ 16{,}848 \\ 28{,}588 \\ 16{,}848 \\ -16{,}848 \\ -16{,}848 \end{array}\right\} \tag{50}$$

and the column axial forces are updated as

$$P_1 = P + (M_5 + M_6)/L_b = 200 + (-16{,}838 - 16{,}838)/240 = 59.6 \text{ kips} \tag{51a}$$

$$P_2 = P - (M_5 + M_6)/L_b = 200 - (-16{,}838 - 16{,}838)/240 = 340.4 \text{ kips} \tag{51b}$$

which remain constant since the moments at M_5 and M_6 remain at their plastic moment capacity. Using Eq. 43a to check for yielding at PHLs #1 and #3 gives

$$\text{PHL \#1:} \quad (59.6/864)^2 + (28884/31104)^2 = 0.867 \tag{52a}$$

$$\text{PHL \#3:} \quad (340.4/864)^2 + (28588/31104)^2 = 1.00 \tag{52b}$$

which indicates that PHL #3 reaches its capacity at this step.

Step 3u: The analysis continues with PHLs #3, #5, and #6 yielded, i.e., $\theta_1'' = \theta_2'' = \theta_4'' = 0$. The lateral force is applied up to $F_o = 535.6$ kips. Rows 1, 2, 3, 6, 8, and 9 are extracted from Eq. 41 with the updated information on the column axial forces obtained in Eq. 51:

$$\left[\begin{array}{ccc:ccc} 126.5 & 5425 & 5397 & 5397 & 0 & 0 \\ 5425 & 1014420 & 203730 & 0 & 407450 & 203730 \\ 5397 & 203730 & 1008100 & 306080 & 203730 & 407450 \\ \hdashline 5397 & 0 & 306080 & 600650 & 0 & 0 \\ 0 & 407450 & 203730 & 0 & 407450 & 203730 \\ 0 & 203730 & 407450 & 0 & 203730 & 407450 \end{array}\right] \left\{\begin{array}{c} x_1 \\ x_2 \\ x_3 \\ \hdashline -\theta_3'' \\ -\theta_5'' \\ -\theta_6'' \end{array}\right\} = \left\{\begin{array}{c} 535.6 \\ 0 \\ 0 \\ \hdashline 28{,}588 \\ -16{,}848 \\ -16{,}848 \end{array}\right\} \tag{53}$$

Solving for the displacements at the DOFs and plastic rotations in Eq. 53 gives

$$\begin{gathered} x_1 = 8.351 \text{ in.} \quad , \quad x_2 = -0.0469 \text{ rad} \quad , \quad x_3 = -0.0446 \text{ rad} \\ \theta_3'' = 0.0047 \text{ rad} \quad , \quad \theta_5'' = -0.0193 \text{ rad} \quad , \quad \theta_6'' = -0.0170 \text{ rad} \end{gathered} \tag{54}$$

Then substituting Eq. 54 back into the last six equations of Eq. 41 gives the moments

$$\left\{\begin{array}{c} M_1 \\ M_2 \\ M_3 \\ M_4 \\ M_5 \\ M_6 \end{array}\right\} = \left[\begin{array}{cccccc} 5425 & 304490 & 0 & 0 & 0 & 0 \\ 5425 & 606970 & 0 & 0 & 0 & 0 \\ 5397 & 0 & 306080 & 600650 & 0 & 0 \\ 5397 & 0 & 600650 & 306080 & 0 & 0 \\ 0 & 407450 & 203730 & 0 & 407450 & 203730 \\ 0 & 203730 & 407450 & 0 & 203730 & 407450 \end{array}\right] \left\{\begin{array}{c} 8.351 \\ -0.0469 \\ -0.0446 \\ -0.0047 \\ 0.0193 \\ 0.0170 \end{array}\right\} = \left\{\begin{array}{c} 31{,}030 \\ 16{,}848 \\ 28{,}588 \\ 16{,}848 \\ -16{,}848 \\ -16{,}848 \end{array}\right\} \tag{55}$$

and the column axial forces remain constant at $P_1 = 59.6$ kips and $P_2 = 340.4$ kips. Using Eq. 43a to check for yielding at PHLs #1 and #3 gives

$$\text{PHL \#1:} \quad (59.6/864)^2 + (31030/31104)^2 = 1.00 \tag{56a}$$

$$\text{PHL \#3:} \quad (340.4/864)^2 + (28588/31104)^2 = 1.00 \tag{56b}$$

which indicates PHL #1 has reached its capacity and PHL #3 has continued yielding at this step. Now that a mechanism has been formed, the frame will continue to deflect without any additional load, and the pushover curve can be plotted as shown in Fig. 6 for the case where geometric nonlinearity are updated due to the change in axial forces in the columns.

Now consider the case where geometric nonlinearity is not updated when there is a change in the column axial forces. This is achieved by using constant stiffness matrices $\mathbf{K}$, $\mathbf{K}'$, and $\mathbf{K}''$ that are computed based on the initial column axial forces throughout the analysis. Using the same one-story frame as shown in Fig. 5, Step 1 above remains the same as previously computed, where $F_o = 484.4$ kips and $x_1 = 6.189$ in., with moments M_5 and M_6 both reaching their moment capacities and $P_1 = P_2 = 200$ kips.

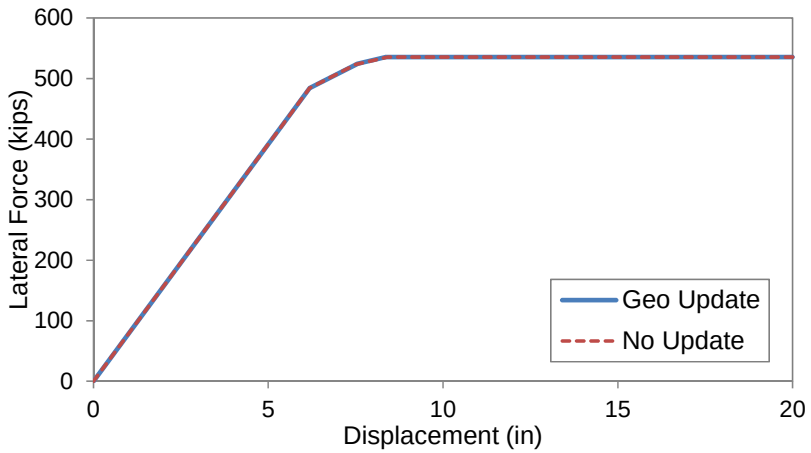

Figure 6: Comparison of pushover curves with and without updates on stiffness due to geometric nonlinearity

Step 2n: The analysis continues with PHLs #5 and #6 yielded, i.e., $\theta_1'' = \theta_2'' = \theta_3'' = \theta_4'' = 0$. The lateral force is applied up to $F_o = 523.0$ kips. Rows 1, 2, 3, 8, and 9 are extracted from Eq. 41 with the axial forces in the columns remain at $P_1 = P_2 = 200$ kips for the purpose of determining the nonlinear geometric stiffness (i.e., update of the geometric nonlinearity is ignored):

$$\left[\begin{array}{ccc:cc} 126.5 & 5411 & 5411 & 0 & 0 \\ 5411 & 1011300 & 203730 & 407450 & 203730 \\ 5411 & 203730 & 1011300 & 203730 & 407450 \\ \hdashline 0 & 407450 & 203730 & 407450 & 203730 \\ 0 & 203730 & 407450 & 203730 & 407450 \end{array}\right] \left\{\begin{array}{c} x_1 \\ x_2 \\ x_3 \\ \hdashline -\theta_5'' \\ -\theta_6'' \end{array}\right\} = \left\{\begin{array}{c} 523.0 \\ 0 \\ 0 \\ \hdashline -16{,}848 \\ -16{,}848 \end{array}\right\} \tag{57}$$

Solving for the displacements at the DOFs and plastic rotations in Eq. 57 gives

$$x_1 = 7.502 \text{ in.} \quad , \quad x_2 = x_3 = -0.0393 \text{ rad} \quad , \quad \theta_5'' = \theta_6'' = -0.0118 \text{ rad} \tag{58}$$

Then substituting Eq. 58 back into the last six equations of Eq. 41 gives the moments

$$\left\{\begin{array}{c} M_1 \\ M_2 \\ M_3 \\ M_4 \\ M_5 \\ M_6 \end{array}\right\} = \left[\begin{array}{ccccc} 5411 & 305280 & 0 & 0 & 0 \\ 5411 & 603820 & 0 & 0 & 0 \\ 5411 & 0 & 305280 & 0 & 0 \\ 5411 & 0 & 603820 & 0 & 0 \\ 0 & 407450 & 203730 & 407450 & 203730 \\ 0 & 203730 & 407450 & 203730 & 407450 \end{array}\right] \left\{\begin{array}{c} 7.502 \\ -0.0393 \\ -0.0393 \\ 0.0118 \\ 0.0118 \end{array}\right\} = \left\{\begin{array}{c} 28{,}588 \\ 16{,}848 \\ 28{,}588 \\ 16{,}848 \\ -16{,}848 \\ -16{,}848 \end{array}\right\} \tag{59}$$

Since both M_5 and M_6 remain at their moment capacities, the column axial forces remain constant at $P_1 = 59.6$ kips and $P_2 = 340.4$ kips. Now using Eq. 43a to check for yielding at PHLs #1 and #3 gives

$$\text{PHL \#1:} \quad (59.6/864)^2 + (28588/31104)^2 = 0.850 \tag{60a}$$

$$\text{PHL \#3:} \quad (340.4/864)^2 + (28588/31104)^2 = 1.00 \tag{60b}$$

which indicates that PHL #3 reaches its capacity at this step.

Step 3n: The analysis continues with PHLs #3, #5, and #6 yielded, i.e., $\theta_1'' = \theta_2'' = \theta_4'' = 0$. The lateral force is applied up to $F_o = 535.4$ kips. Rows 1, 2, 3, 6, 8, and 9 are extracted from Eq. 41 with the axial forces in the columns remain at $P_1 = P_2 = 200$ kips for the purpose of determining the nonlinear geometric stiffness:

$$\left[\begin{array}{cccccc} 126.5 & 5411 & 5411 & 5411 & 0 & 0 \\ 5411 & 1011300 & 203730 & 0 & 407450 & 203730 \\ 5411 & 203730 & 1011300 & 305280 & 203730 & 407450 \\ \hline 5411 & 0 & 305280 & 603820 & 0 & 0 \\ 0 & 407450 & 203730 & 0 & 407450 & 203730 \\ 0 & 203730 & 407450 & 0 & 203730 & 407450 \end{array}\right] \left\{\begin{array}{c} x_1 \\ x_2 \\ x_3 \\ \hline -\theta_3'' \\ -\theta_5'' \\ -\theta_6'' \end{array}\right\} = \left\{\begin{array}{c} 535.4 \\ 0 \\ 0 \\ \hline 28{,}588 \\ -16{,}848 \\ -16{,}848 \end{array}\right\} \tag{61}$$

Solving for the displacements at the DOFs and plastic rotations in Eq. 61 gives

$$\begin{gathered} x_1 = 8.414 \text{ in.} \quad , \quad x_2 = -0.0475 \text{ rad} \quad , \quad x_3 = -0.0448 \text{ rad} \\ \theta_3'' = 0.0054 \text{ rad} \quad , \quad \theta_5'' = -0.0199 \text{ rad} \quad , \quad \theta_6'' = -0.0172 \text{ rad} \end{gathered} \tag{62}$$

Then substituting Eq. 62 back into the last six equations of Eq. 41 gives the moments

$$\left\{\begin{array}{c} M_1 \\ M_2 \\ M_3 \\ M_4 \\ M_5 \\ M_6 \end{array}\right\} = \left[\begin{array}{cccccc} 5411 & 305280 & 0 & 0 & 0 & 0 \\ 5411 & 603820 & 0 & 0 & 0 & 0 \\ 5411 & 0 & 305280 & 603820 & 0 & 0 \\ 5411 & 0 & 603820 & 305280 & 0 & 0 \\ 0 & 407450 & 203730 & 0 & 407450 & 203730 \\ 0 & 203730 & 407450 & 0 & 203730 & 407450 \end{array}\right] \left\{\begin{array}{c} 8.414 \\ -0.0475 \\ -0.0448 \\ -0.0054 \\ 0.0199 \\ 0.0172 \end{array}\right\} = \left\{\begin{array}{c} 31{,}030 \\ 16{,}848 \\ 28{,}588 \\ 16{,}848 \\ -16{,}848 \\ -16{,}848 \end{array}\right\} \tag{63}$$

and the column axial forces remain constant at $P_1 = 59.6$ kips and $P_2 = 340.4$ kips. Using Eq. 43a to check for yielding at PHLs #1 and #3 gives

$$\text{PHL \#1:} \quad (59.6/864)^2 + (31030/31104)^2 = 1.00 \tag{64a}$$

$$\text{PHL \#3:} \quad (340.4/864)^2 + (28588/31104)^2 = 1.00 \tag{64b}$$

which indicates PHL #1 has reached its capacity and PHL #3 has continued yielding at this step. Now that a mechanism has been formed, the frame will continue to deflect without any additional load, and the pushover curve can be plotted as shown in Fig. 6 for the case where the update of stiffness matrix due to geometric nonlinearity is ignored when axial forces in the columns change.

Fig. 6 shows that the difference between whether or not to update the geometric nonlinearity due to

changes in column axial force at every step on the pushover curve is negligible. One hidden assumption often made among various software packages, including Perform-3D (CSI 2011a), is that the effect of changing axial force in the frame on the geometric stiffness matrices is ignored, and therefore the geometric nonlinearity need not be updated. The idea behind this assumption is that when lateral displacement imposes overturning moment on the entire framed structure, global equilibrium requires that there will be an increase in column compression on one side of the frame and an equal amount of reduction in column compression on the opposite side of the frame. While an increase in column compression on one side of the frame reduces the lateral stiffness of these columns, a reduction in column compression on the opposite side of the frame increases the lateral stiffness of those columns by a similar amount. The end result is that the net change in total lateral stiffness of the entire frame becomes negligible, and this can be observed when the stiffness matrix in Eq. 48 (**Step 2u**) is compared with that in Eq. 57 (**Step 2n**). Similar observations can also be made when the stiffness matrix in Eq. 53 (**Step 3u**) is compared with that in Eq. 61 (**Step 3n**). Therefore, an assumption to keep the geometrically nonlinear stiffness matrices unchanged throughout the analysis, even as loading increases, is reasonable.

6. Pushover Analysis of a Two-Story Frame

Consider the two-story moment-resisting steel frame as shown in Fig. 7. Assume that axial deformation is ignored for the beam members, this gives a system with 17 DOFs ($n=17$) and 17 PHLs ($m=17$), resulting in a 17×17 $\mathbf{K}$ matrix, a 17×17 $\mathbf{K}'$ matrix, and a 17×17 $\mathbf{K}''$ matrix. Let $E=0.9\times29000=26{,}100$ ksi be the elastic modulus and $f_Y=0.9\times36=32.4$ ksi be the yield stress of steel. Also, let the yielding surface of the column plastic hinges be

$$\begin{cases} \dfrac{P_k}{f_Y A_{ck}}+\dfrac{8}{9}\left(\dfrac{M_k}{f_Y Z_{ck}}\right)=1.0 \quad if \ \dfrac{P_k}{f_Y A_{ck}}\geq 0.2 \\ \dfrac{P_k}{2 f_Y A_{ck}}+\left(\dfrac{M_k}{f_Y Z_{ck}}\right)=1.0 \quad if \ \dfrac{P_k}{f_Y A_{ck}}< 0.2 \end{cases} \qquad k=1,...,9 \tag{65}$$

where P_k is the axial force, M_k is the plastic hinge moment, A_{ck} is the cross-sectional area, and Z_{ck} is the plastic section modulus of the column containing the kth plastic hinge.

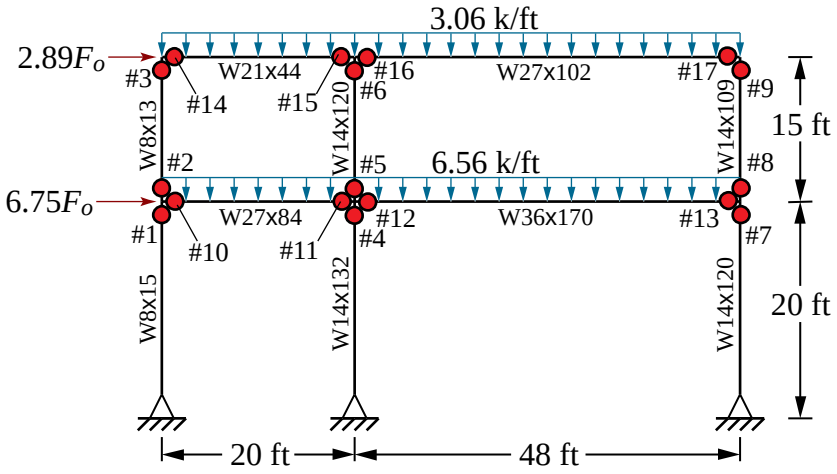

Figure 7: Two-story moment-resisting steel frame

Step 1: The analysis begins with considering the gravity loads only. The frame is assumed to respond in the linearly elastic range. At an applied lateral force of $F_o = 0$, the responses and the column axial forces are calculated, and the resulting roof displacement is $x_2 = -0.437$ in.

Step 2: The analysis continues with an addition of the applied lateral forces. At this point, the frame is assumed to remain in the linearly elastic range, i.e., $\theta_1'' = \theta_2'' = ... = \theta_{17}'' = 0$. The lateral force is now applied up to $F_o = 2.05$, giving a base shear of $V = 19.76$ kips. Without considering any update on the axial force due to geometric nonlinearity, the resulting roof displacement is $x_2 = 1.369$ in. and a plastic hinge at PHL #11 is formed at this applied lateral force level.

Step 3n: The analysis continues with an increase of the applied lateral forces and a plastic hinge at PHL #11, i.e., $\theta_1'' = ... = \theta_{10}'' = 0$ and $\theta_{12}'' = ... = \theta_{17}'' = 0$. The lateral force is now applied up to $F_o = 3.05$, giving a base shear of $V = 29.40$ kips. By solving the matrix equation with 18 unknowns (17 DOFs plus 1 PHL), the resulting roof displacement is calculated as $x_2 = 2.318$ in. At this point, a plastic hinge at PHL #7 is formed, and the plastic rotation at PHL #11 is $\theta_{11}'' = -0.00059$ rad.

Step 4n: The analysis continues with an increase of the applied lateral forces and plastic hinges at PHLs #7 and #11, i.e., $\theta_1'' = ... = \theta_6'' = 0$, $\theta_8'' = \theta_9'' = \theta_{10}'' = 0$, and $\theta_{12}'' = ... = \theta_{17}'' = 0$. The lateral force is now applied up to $F_o = 4.10$, giving a base shear of $V = 39.52$ kips. By solving the matrix equation with 19 unknowns (17 DOFs plus 2 PHLs), the resulting roof displacement is now calculated as $x_2 = 4.776$ in. At this point, a plastic hinge at PHL #4 is formed, and the plastic rotations at the other PHLs are $\theta_7'' = 0.01018$ rad and $\theta_{11}'' = -0.00255$ rad.

Step 5n: The analysis continues with an increase of the applied lateral loads and plastic hinges at PHLs #4, #7, and #11, i.e., $\theta_1'' = \theta_2'' = \theta_3'' = \theta_5'' = \theta_6'' = \theta_8'' = \theta_9'' = \theta_{10}'' = 0$ and $\theta_{12}'' = ... = \theta_{17}'' = 0$. The lateral force is now reduced to $F_o = 3.71$, giving a base shear of $V = 35.76$ kips. By solving the matrix equation with 20 unknowns (17 DOFs plus 3 PHLs), the resulting roof displacement is now calculated as $x_2 = 6.114$ in. At this point, a plastic hinge at PHL #1 is formed, and the plastic rotations the other PHLs are $\theta_4'' = 0.00576$ rad, $\theta_7'' = 0.01596$ rad, and $\theta_{11}'' = -0.00256$ rad.

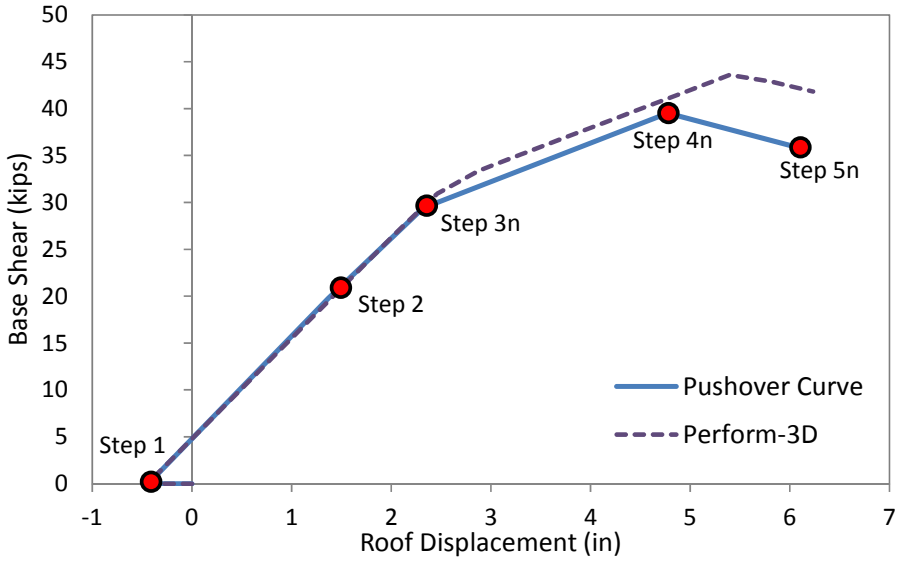

Figure 8: Pushover curve of a two-story frame without update of geometric nonlinearity

The analysis stops at this point, which is when a mechanism is formed with PHLs #1, #4, and #7 yielded. The resulting pushover curve is shown in Fig. 8, and a similar curve obtained using Perform-3D is also plotted in the figure as a comparison. While Perform-3D also shows only PHLs #1, #4, #7, and #11 have yielded, the difference between the two curves after yielding can be attributed to the default column yield surface in Perform-3D that is different from the one defined in Eq. 65. Note that the present analysis is able to easily capture the strain softening response of the structure as shown in Fig. 8, which is one of the major advantages of the FAM.

7. Conclusions

In this paper, a detailed derivation of the nonlinear geometric stiffness matrices using stability functions was presented on a column member with plastic hinges at the ends. Through this derivation, it was demonstrated that the stiffness force can be computed by simply multiplying a geometric nonlinear stiffness matrix with a material nonlinear displacement vector. While the use of stability functions produced the global stiffness matrix that was numerically equivalent to the common use of geometric stiffness approach, using stability functions was demonstrated through numerical calculation to have the advantage of capturing the P-δ effect exactly. This results in the simplicity on incorporation of the force analogy method for addressing material nonlinearity into the formulation and the accuracy when static condensation is performed. Numerical examples using one-story and two-story frames were then presented to show the simplicity of the method for analyzing the responses of nonlinear framed structures. Through these numerical exercises, it was demonstrated that updating the geometric stiffness is not a major factor on influencing the shape of the pushover curves.

8. Disclaimers

Certain software may have been identified in this paper in order to specify the analytical procedure adequately. Such identification is not intended to imply recommendation or endorsement by the National Institute of Standards and Technology (NIST), nor is it intended to imply that the software identified are necessarily the best available for the purpose.

The policy of NIST is to use the International System of Units (metric units) in all publications. In this document, however, some information is presented in the U.S. Customary Units, as this is the U.S. earthquake engineering industry preferred system of units.

References

Bazant, Z.P., Cedolin, L. (2003). *Stability of Structures*, Dover Publication, New York.

Computers and Structures, Inc. (2011a). Perform-3D Version 5.0.0, *Nonlinear Analysis and Performance Assessment of 3D Structures*, Berkeley, California.

Computers and Structures, Inc. (2011b). SAP2000 Version 15.1.0, *Integrated Software for Structural Analysis and Design*, Berkeley, California.

Horne, M.Z., Merchant, W. (1965). *The Stability of Frames*, Pergamon Press, New York.

McGuire, W., Gallagher, R.H., Ziemian, R.D. (2000). *Matrix Structural Analysis*, John Wiley and Sons, New York.

Park, J.W., Kim, S.E. (2008). "Nonlinear inelastic analysis of steel-concrete composite beam-columns using the stability functions." *Structural Engineering and Mechanics*, 30 (6) 763-785.

Powell, G.H. (2010). *Modeling for Structural Analysis - Behavior and Basics*, Computer and Structures Inc., Berkeley, California.

Timoshenko, S.P., Gere, J.M. (1961). *Theory of Elastic Stability, 2nd Edition*, McGraw Hill, New York.

Wilson, E. (2002). *Three-Dimensional Static and Dynamic Analysis of Structures - A Physical Approach with Emphasis on Earthquake Engineering, 3rd Edition*, Computer and Structures Inc., Berkeley, California.

Wong, K.K.F., Yang, R. (1999). "Inelastic dynamic response of structures using force analogy method." *Journal of Engineering Mechanics ASCE*, 125 (10) 1190-1199.